INTERNATIONAL JOURNAL FOR NUMERICAL METHODS IN FLUIDS, VOL. 17, 1–22 (1993)

NUMERICAL SOLUTIONS OF A NON-LINEAR DENSITY CURRENT: A BENCHMARK SOLUTION AND COMPARISONS

J. M. STRAKA

School of Meteorology, University of Oklahoma, Energy Center, Room 1310, 100 East Boyd Street, Norman, OK 73019, U.S.A.

ROBERT B. WILHELMSON AND LOUIS J. WICKER

University of Illinois, Urbana, IL 61801, U.S.A.

JOHN R. ANDERSON

University of Wisconsin, Madison, WI 53706, U.S.A.

AND

KELVIN K. DROEGEMEIER

University of Oklahoma, Norman, OK 73019, U.S.A.

SUMMARY

A comparison between solutions from simulations of a non-linear density current test problem was made in order to study the behaviour of a variety of numerical methods. The test problem was diffusion-limited so that a grid-converged reference solution could be generated using high spatial resolution. Solutions of the test problem using several different resolutions were computed by the participants of the 'Workshop on Numerical Methods for Solving Nonlinear Flow Problems', which was held on 11–13 September 1990 at the National Center for Supercomputing Applications (NCSA). In general, it was found that when the flow was adequately resolved, all of the numerical schemes produced solutions that contained the basic physics as well as most of the flow detail of the reference solution. However, when the flow was marginally resolved, there were significant differences between the solutions produced by the various models. Finally, when the flow was poorly resolved, none of the models performed very well. While higher-order and spectral-type schemes performed best for adequately and marginally resolved flow, solutions made with these schemes were virtually unusable for poorly resolved flow. In contrast, the monotonic schemes provided the most coherent and smooth solutions for poorly resolved flow, however with noticeable amplitude and phase speed errors, even at finer resolutions.

KEY WORDS Navier–Stokes Density current Converged solution Nonlinear Richardson extrapolation Numerical methods

1. INTRODUCTION

Many numerical techniques have been developed during the past 35 years to solve the Navier–Stokes equations for initial boundary value problems of non-linear fluid flow. Some of these techniques have been designed for specific types of problems such as shock waves, while

0271–2091/93/130001–22$16.00

Received 18 March 1992
Revised 12 January 1993

others have been developed to improve global conservation of various fluid properties and accuracy in the details of the simulated flow. However, no scheme has ever been proven superior for universal application.

The wide acceptance of the many different types of numerical schemes that have been developed is based on their usefulness in simulating particular non-linear fluid flow problems, and is rooted in the proof of theorems such as those developed by Lax, which state that consistency and stability are the necessary and sufficient conditions for convergence of linear problems.[1] Thus, given a stable and consistent difference form of a continuous system, a grid-converged* solution can be obtained as Δx and $\Delta t \rightarrow 0$. This implies that all stable and consistent difference systems for a given linear continuous system should approach the same grid-converged or analytic solution.

In the past, only a modest number of papers in the literature have been devoted to studying systematically the behaviour of the many types of numerical techniques applied to multidimensional non-linear problems.[2,3] One reason for this is that it has been very difficult until recently to obtain grid-converged solutions for these problems. Computers now have enough speed and memory so that grid-converged numerical solutions can be found for non-linear problems with scale-limiting physics, such as diffusion, by using very high resolution. However, there is generally no agreement in the literature as to what problems are best suited for testing various numerical techniques. As a result, researchers generally choose test problems that have relevance to their fields of study,[4,5] or are much simpler than the real problems of interest. While this has proven useful for individual disciplines, it makes comparisons of the behaviour of various numerical techniques difficult.

With this in mind, a 'Workshop on Numerical Methods for Solving Nonlinear Flow Problems' was held† on 11–13 September 1990 at the National Center for Supercomputing Applications (NCSA) to study the behaviour of a variety of numerical methods when applied to a particular diffusion-limited‡ non-linear test problem of fluid flow for which a grid-converged solution could be generated. The workshop was designed to be a forum for discussion of a variety of traditional and new numerical methods in the context of their use in solving non-linear systems of equations encountered in atmospheric science, astrophysics, aerodynamics, turbulence and other fluid flow disciplines. Researchers were requested to use the numerical methods that they had developed (or were developing) to generate solutions at various resolutions for a prescribed fluid flow test problem, and invited to describe their results in oral presentations§, ¶ at the workshop. Some of

* The term grid-converged is used to state that no meaningful improvement in a numerical solution could be obtained using higher resolution within the practical limits of finite precision, speed and memory of a computing machine.

† The workshop was held at the National Center for Supercomputing Applications (NCSA) at the University of Illinois, and was co-sponsored by the NCSA, the Space Science and Engineering Center (SSEC) at the University of Wisconsin and the Center for Analysis and Prediction of Storms (CAPS) at the University of Oklahoma.

‡ In the numerical simulation of diffusion-limited problems, the length scale of the smallest resolvable flow features is dictated by the length scale associated with the diffusion.

§ Numerical scheme presentations were made by Dr. John Anderson (SSEC, University of Wisconsin), Richard Carpenter (CAPS, University of Oklahoma), Dr. Stevens Chan (LLNL, University of California), Dr. Scott Fulton (Clarkson University), Dr. Wojciech Grabowski (NCAR), Dr. John Hawley (University of Virginia), Dr. Mike Norman (NCSA, University of Illinois), Dr. Jim Stone (NCSA, University of Illinois), Dr. Vic Ooyama (AOML), Dr. Miodrag Rancic (CAPS, University of Oklahoma), Dr. William Skamarock (NCAR), Dr. Piotr Smolarkiewicz (NCAR), Dr. Jerry Straka (University of Oklahoma), Dr. Greg Tripoli (University of Wisconsin), Dr. Louis Wicker (NCSA, University of Illinois) and Dr. Ming Xue (CAPS, University of Oklahoma). Drs. Anderson, Straka and Wilhelmson opened the workshop with a discussion of the reference solution.

¶ Presentations were made by Dr. Larry Smarr (NCSA) on the High Performance Computing Initiative, Dr. John Anderson (SSEC) on Parallel Computing, Matt Arrott (NCSA) on Distributed Computing and Visualization, Charlie Catlett (NCSA) on Networking, Dr. Mike Norman (NCSA) on the Scientific Workbench and Dr. Kelvin Droegemeier (CAPS), Dr. Bill Skamarock (NCAR), Dr. Bob Wilhelmson (NCSA) and Dr. Jim Stone (NCSA) on Visualization.

the numerical methods used by the workshop participants include traditional finite differences, piecewise polynomial approximations, grid adaptation, and local and global spectral techniques. It is important to note that the primary emphasis of the workshop was to examine the behaviour of various numerical schemes, not to determine the most economical and most accurate numerical schemes.

In this paper, selected results from the workshop are presented to illustrate the behaviour of solutions from several different numerical methods for resolutions that poorly, marginally and accurately resolved the basic evolution and flow features of the test problem. The criteria that were used to select an appropriate test problem together with the governing equations, boundary conditions and initial conditions are presented in Section 2. Next, results from a grid-converged solution of the test problem are described in Section 3. This solution was used to gauge the accuracy of the solutions provided by the invited researchers. Then, results from the application of these different numerical techniques to the test problem are described in Section 4. Finally, a summary of the results and conclusions from the workshop are presented in Section 5.

2. TEST PROBLEM

There are many interesting two- and three-dimensional non-linear fluid flow problems that could have been chosen for the workshop. A two-dimensional problem was chosen as most of the researchers invited to the workshop had two-dimensional models. In addition, it was more computationally feasible to obtain a grid-converged solution for a two-dimensional problem than for a three-dimensional problem. In order to obtain a grid-converged solution, the problem necessarily had to be diffusion-limited. To test the robustness of a variety of numerical methods, a test problem was designed that contained non-linear dynamics, transient features and fine-scale structures. Finally, it was required that the problem was simple to implement, utilized Cartesian co-ordinates, was solvable using both compressible and incompressible flow equations, and contained minimal 'non-dynamical' physics so that researchers from any discipline studying fluid flow could participate without making major source code changes to their hydrodynamic models.

After careful consideration and experimentation, a density current problem in an otherwise homogeneous and isentropic two-dimensional fluid was chosen that was similar to that used in the study reported by Droegemeier and Wilhelmson.[6] The density current was initiated as a cold blob of air that subsequently descended to the ground. As the density current spread out laterally at the lower boundary, Kelvin–Helmholtz shear instability rotors formed along the top of the cold air boundary (Figure 1).

The fully compressible equations for fluid flow that describe the density current problem are as follows:

mass continuity

$$(\rho)_t+(\rho u)_x+(\rho w)_z=0,$$

horizontal momentum

$$(\rho u)_t+(\rho uu)_x+(\rho uw)_z+p_x-\rho K(u_{xx}+u_{zz})=0,$$

vertical momentum

$$(\rho w)_t+(\rho uw)_x+(\rho ww)_z+p_z+\rho g-\rho K(w_{xx}+w_{zz})=0,$$

energy

$$(\varepsilon\rho)_t+(\varepsilon\rho u)_x+(\varepsilon\rho w)_z+p(u_x+w_z)-K\rho T(C_p\theta^{-1})(\theta_{xx}+\theta_{zz})=K\rho T(C_p\theta^{-1})[(\theta)_t+u(\theta)_x+w(\theta)_z],$$

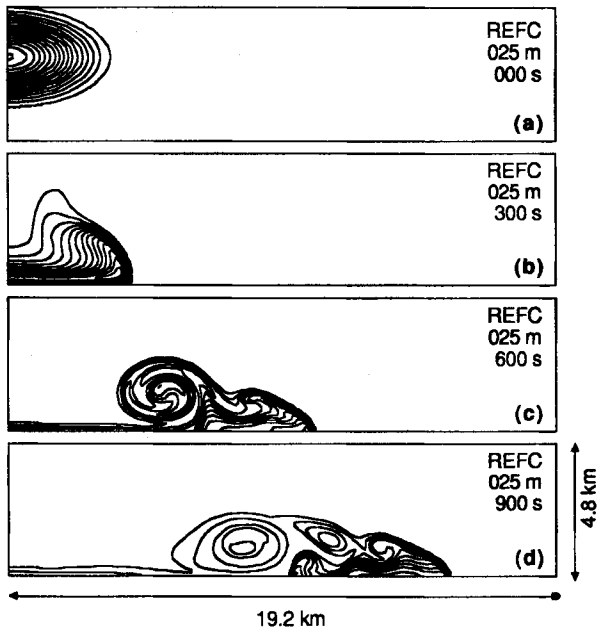

Figure 1. Plots of θ' at (a) 0, (b) 300, (c) 600 and (d) 900 s for the 25·0 m resolution compressible reference model solution. Contour interval (CI) is 1°C and the contours are centred around 0°C. The minimum value of θ' at 0 s is −16·624°C (note that only the lower left 0·75 of the domain is shown)

equation of state

$$P=\rho R_d T,$$

internal energy

$$\varepsilon=C_v T,$$

exner function

$$\pi=(pp_0^{-1})^{R_d/C_p}.$$

In the above equations, u is the horizontal velocity, w the vertical velocity, ρ the density, p the pressure, ε the energy and θ the potential temperature. The independent variables are horizontal (x) and vertical (z) Cartesian grid directions, and time (t). Variables and quantities subscripted with t, x and z are derivatives with respect to the independent variables. Other constants include: $R_d=287{\cdot}0\ \mathrm{J\,kg^{-1}\,K^{-1}}$ (gas constant for dry air); $C_p=1004{\cdot}0\ \mathrm{J\,kg^{-1}\,K^{-1}}$ (specific heat at constant pressure); $C_v=717{\cdot}0\ \mathrm{J\,kg^{-1}\,K^{-1}}$ (specific heat at constant volume); $p_0=100\,000{\cdot}0\ \mathrm{kg\,m^{-1}\,s^{-2}}$ (reference pressure); $g=9{\cdot}81\ \mathrm{m\,s^{-2}}$ (gravitational parameter); $K=75{\cdot}0\ \mathrm{m^2\,s^{-1}}$ (diffusion coefficient); $T_s=\theta=300{\cdot}0$ K (surface temperature). Finally, temperature is defined as $T=\pi\theta$.

Approximations of the compressible system described above can also be used to integrate the model test problem since the flow velocities are well below the speed of sound. For example, in the anelastic system there is no tendency equation for density,[7] and the mass continuity equation is

$$(\bar{\rho}u)_x+(\bar{\rho}w)_z=0,$$

where base state variables are a function of only z and are denoted by an overbar. In the anelastic system, only the base state density is considered, except when coupled with gravity. Furthermore,

the pressure is computed from a diagnostic pressure equation obtained by differencing the u and w momentum equations with respect to x and z, respectively. In the quasi-compressible system (super-compressible system), a pressure tendency is used.[8-10] This tendency equation is approximated by

$$(p-\bar{p})_t = p'_t = -c_s^2[(\bar{\rho}u)_x + (\bar{\rho}w)_z],$$

where c_s is the pseudo sound speed, and primed variables are perturbations from the base state. For example, p' is given as $p'=(p-\bar{p})$. As with the anelastic system, only the base state density is used in the quasi-compressible system, except when density is coupled with gravity. Both Anderson *et al.*[9] and Droegemeier and Davies-Jones[10] have shown that the quasi-compressible system produces accurate solutions provided that c_s is at least twice the speed of the fastest physically important signal in the system. In addition, Anderson *et al.*[9] and Chorin[8] have shown that the quasi-compressible system approaches the anelastic system in the limit as $c_s \to \infty$.

The lateral boundary conditions for the test problem are $u = w_x = p_x = \theta_x = 0$, and the vertical boundary conditions are $w = u_z = p_z = \theta_z = 0$. For real atmospheric problems, the vertical pressure gradient at the upper and lower boundaries would typically follow from the vertical equation of motion, with $w=0$ at the vertical boundaries. To simplify the test problem, a reflective condition is applied to p at the upper and lower boundaries and the gravitational parameter changes sign below $z=0$ and above $z=6{\cdot}4$ km. Also, note that a free slip condition on the velocity components is imposed at the walls of the domain.

The dependent variables are initialized by their base state values, which are a function of z, as:

$$\bar{T} = T_s - zgC_p^{-1}, \qquad \bar{p} = p_0(\bar{T}T_s^{-1})^{R_d/C_p},$$

$$\bar{\rho} = \bar{p}(R_d\bar{T})^{-1}, \qquad \frac{d\bar{p}}{dz} = -\bar{\rho}g,$$

$$\bar{\theta} = T_s = 300\,\text{K}, \qquad u = v = 0{\cdot}0.$$

To provide the negative buoyancy necessary to initiate a density current, the following function is used to specify a temperature perturbation:

$$\Delta T = \begin{cases} 0{\cdot}0\,^\circ\text{C} & \text{if } L > 1{\cdot}0, \\ -15{\cdot}0\,^\circ\text{C}[\cos(\pi L)+1{\cdot}0]/2 & \text{if } L \le 1{\cdot}0, \end{cases}$$

where $L = \{[(x-x_c)x_r^{-1}]^2 + [(z-z_c)z_r^{-1}]^2\}^{0{\cdot}5}$, $x_c = 0{\cdot}0$ km, $x_r = 4{\cdot}0$ km, $z_c = 3{\cdot}0$ km and $z_r = 2{\cdot}0$ km. The quantity $\Delta\theta$ can be evaluated from ΔT and the relation $T = \pi\theta$. The minimum temperature in the thermal perturbation is $-15{\cdot}0\,^\circ$C, and it is centred at $x = 0{\cdot}0$ km, which is in the middle of the domain. With the initial and boundary conditions described above, the domain is symmetric about the vertical line at $x = 0{\cdot}0$ km and is periodic over the interval from $-25{\cdot}6$ to $25{\cdot}6$ km. To minimize computational costs, the symmetry of the problem is exploited. A plot of the initial θ' temperature field is shown in Figure 1(a) with the thermal perturbation centred on the symmetric left boundary ($x=0$).

3. REFERENCE SOLUTIONS

To standardize the comparisons of the solutions of the test problem, a set of simulations was made with a fully compressible reference model. This model (hereafter called the REFC model) was integrated using standard second-order centred-in-time and centred-in-space differences on an unstaggered grid (Arakawa A-grid[11]). A time filter was used to prevent the separation of solutions that can occur with centred time differences.[12] The form of this filter is

$\phi^{t^*}=(1-2\alpha)\phi^t+\alpha(\phi^{t-\Delta t}+\phi^{t+\Delta t})$, where ϕ is any prognostic variable and $\alpha=0{\cdot}10$ is the filter coefficient. The advection terms were differenced using a second-order quadratic conserving scheme.[13,14] To maintain linear stability, the diffusion terms were integrated from time $t-\Delta t$ with a forward-in-time differencing scheme. The reference simulations were initiated with a thermal perturbation as described in Section 2, and integrated out to 900 s. A grid-converged solution, or what will now be called the reference solution, was obtained with a grid resolution of 25·0 m. A time step of $1{\cdot}5625\times10^{-2}$ s was used to integrate the REFC solution. The resolution for the reference solution was determined by successively halving the grid resolution in simulations, starting from 400·0 m resolution, until no significant improvement in the solution could be achieved. The accuracy of the 25·0 m reference solution is discussed after discussing the evolution of the density current simulation.

The evolution of the density current in the reference solution can be described in terms of three Kelvin–Helmholtz shear instability rotors that develop along the top boundary of the simulated cold air outflow boundary during the period from 0 to 900 s. The evolution of these rotors can be seen in the θ' solutions from the 25·0 m resolution reference simulation at 0, 300, 600 and 900 s (Figure 1). In addition, the p', θ', u and w fields from the reference simulation at 900 s are shown together in Figure 2. At the beginning of the simulation, a downdraft formed and accelerated in response to the negative buoyancy described by the initial conditions. The initial buoyancy gradient resulted in the production of vorticity that helped force the first rotor before the cold thermal reached the lower boundary. A pressure excess developed at the bottom of the domain where the downdraft was decelerated by the lower boundary, and the accompanying horizontal pressure gradient turned the flow and accelerated it horizontally. By 300 s, the first rotor was well developed, and was near the leading edge of the density current in a region of strong vertical shear

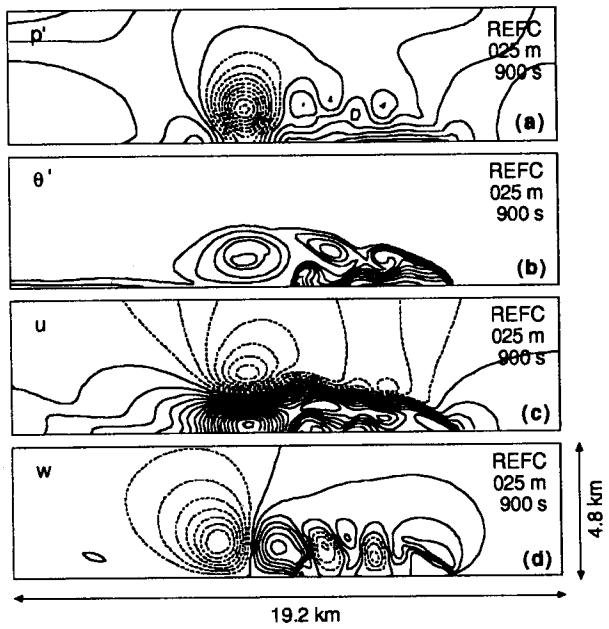

Figure 2. Plots, with contour intervals (CI) given in parentheses, of (a) p' (CI = 0·5 mb), θ' (CI = 1°C), (b) u (CI = 2 m s^{-1}) and (c) w (CI = 2 m s^{-1}) at 900 s for the 25·0 m resolution compressible reference model solution. All contours are centred around zero contours (as in Figure 1)

of the u-wind. At this time, both the peak u-wind and the propagation speed of the front of the density current were more than 30 m s^{-1}. Between 300 and 600 s, the Kelvin–Helmholtz shear instability along the top of the outflow boundary intensified the first rotor, and forced a second rotor to develop at the front of the density current. During this period, the peak outflow wind speed accelerated to 36 m s^{-1}, while the propagation speed of the front slowed to 18 m s^{-1}. By 900 s, a third rotor developed, and the speed of the front slowed further to about 15 m s^{-1}. In simulations carried out beyond 900 s, new rotors formed about every 300 s. For example, the small perturbation on the leading edge of the density current at 900 s evolved into the next rotor. The density current evolution described above is typical of that produced in simulations that assume a constant potential temperature environment with no vertical wind shear.[15,6]

The θ' solutions made with the REFC model at 900 s for various resolutions between 25·0 and 533·3 m are used to help show that a grid-converged solution is obtainable with high enough resolution (Figure 3). In making the solutions shown in Figure 3, the ratio of $\Delta t/\Delta x$ was held constant. By comparing the solutions in Figure 3, it can be seen that all of the simulations are visually distinguishable from the 25·0 m reference solution, except for, perhaps, the 33·3 m solution. Notice that the basic structures of the flow are not resolved until the resolution is at least 133·3 m. The most noticeable differences between the solutions are (1) the propagation speed of the density current, (2) the formation and location of the Kelvin–Helmholtz rotors, and (3) the coherency of the solutions. From the results shown in Figure 3, the basic flow features (e.g. the

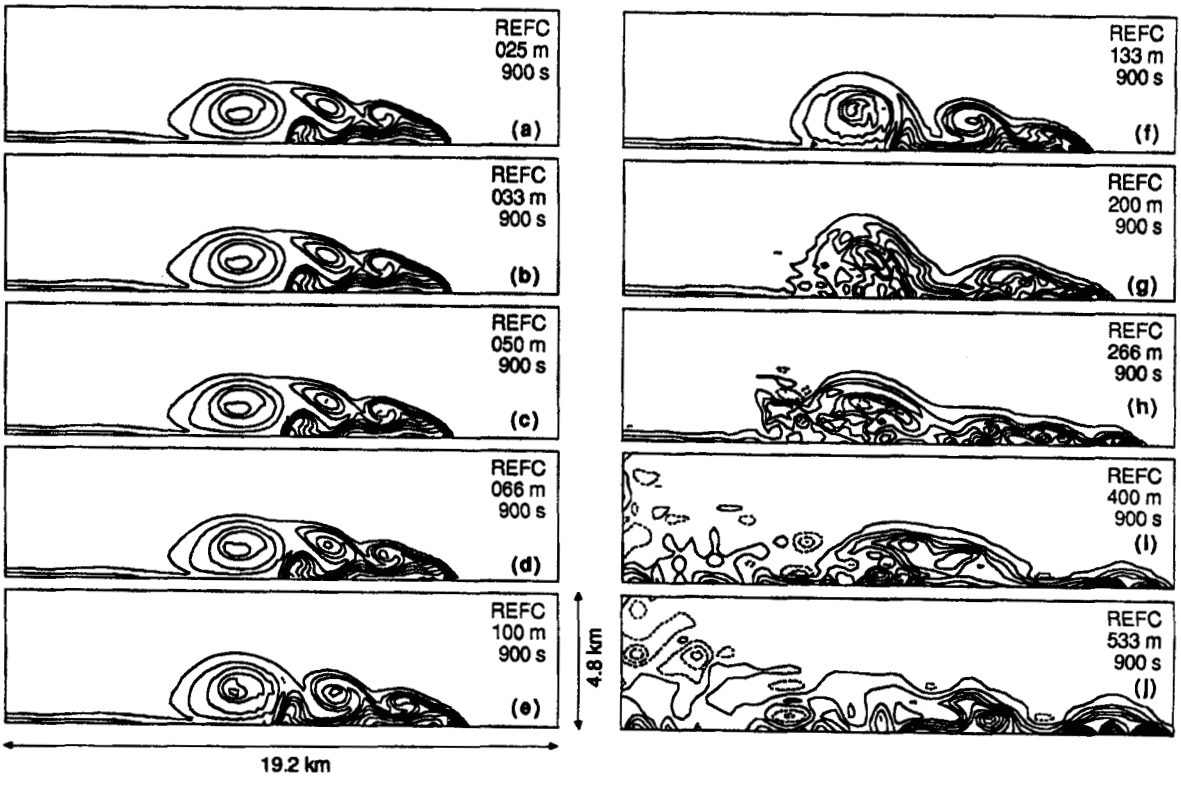

Figure 3. Plots of θ' at 900 s from the compressible reference model using (a) 25·0, (b) 33·3, (c) 50·0, (d) 66·6, (e) 100·0, (f) 133·3, (g) 200·0, (h) 266·6, (i) 400·0 and (j) 533·3 m resolution (as in Figure 1)

three rotors) appear to be adequately resolved at 100·0 m, marginally resolved at 200·0 m, and poorly resolved at 400·0 m resolution.

To quantify the errors in the solutions from the REFC model, the L_2 norm of θ' is computed with

$$L_2(\theta') = \left\{ \frac{1}{\mathrm{NX\,NZ}} \sum_{i=1}^{\mathrm{NX}} \sum_{k=1}^{\mathrm{NZ}} [\theta'(x_i, z_k) - \theta'_{\mathrm{ref}}(x_{ii}, z_{kk})]^2 \right\}^{0.5},$$

where NX and NZ are the number of grid points in any particular solution, i and k are the grid indices in the particular solution, and ii and kk are the grid locations in the 25·0 m reference solution that correspond to i and k.

A plot showing the results of the L_2 norm computations for the θ' solutions made with Δt = constant (the Δt for the 25·0 m reference solution) is shown in Figure 4. The lines in Figure 4 labelled with $O(1)$ and $O(2)$ indicate the slopes of first- and second-order convergence, respectively. (The behaviour of the L_2 norms for u, w and p' is essentially identical to that for the L_2 norms for θ'.) At coarse resolutions ($\Delta x > 133{\cdot}0$ m) the convergence is barely first-order, despite the fact that a second-order-accurate model is used. This is because the basic features of the flow are underresolved at these resolutions. Convergence finally improves to second-order for resolutions less than 133·0 m, which is consistent with the visual analysis of the θ' solutions described

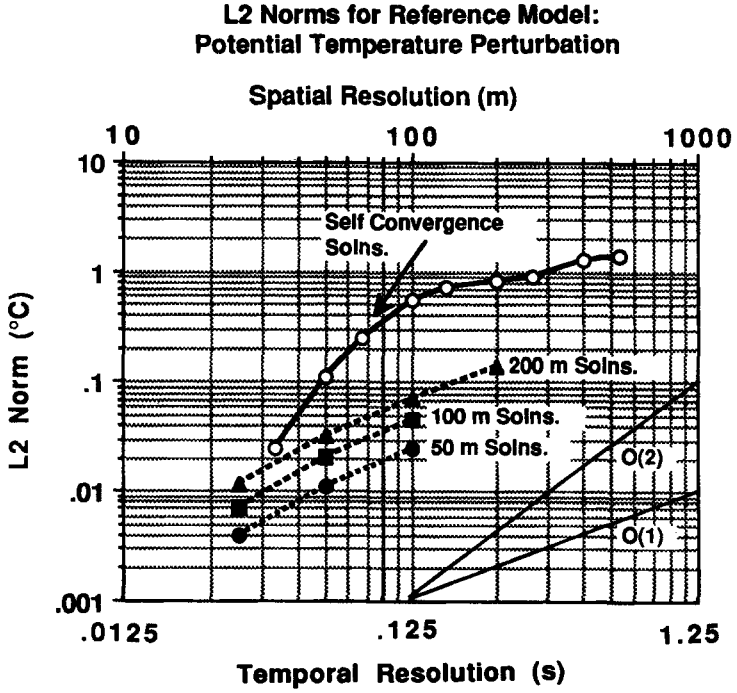

Figure 4. Graph of θ' L_2 norms (°C) from self-convergence tests with the compressible reference model (REFC). The bold solid line labelled with 'self-convergence solutions' represents the L_2 norms for spatial truncation errors of solutions made with Δt = constant and varying grid spacings. The L_2 norms were computed against a 25·0 m reference solution. The bold dashed lines labelled with, for example, '200·0 m solutions' represent L_2 norms for temporal truncation errors of solutions made with Δx = constant (e.g. 200·0 m) and varying time steps. The reference solutions for these computations were made using a time step consistent with $\Delta t = 12{\cdot}5$ s times a constant (see text) in each of the cases. The solid lines labelled $O(1)$ and $O(2)$ represent first- and second-order convergence, respectively

above. Note that the smallest scale features are barely resolved by five grid points with 100·0 m resolution, while they are well resolved by about 20 grid points with 25·0 m resolution. The L_2 norms for θ', at higher resolutions, are small (in a relative sense), suggesting that spatial truncation errors are small and that higher resolution will not result in a better solution. Additional simulations were also made with resolutions as fine as 12·5 and 8·33 m, but in a smaller domain (19·2 × 4·8 km) for computational reasons. As expected, these solutions were essentially identical to the 25·0 m reference solution described above (suggesting, also, the minimal impact of domain size on the solutions).

Richardson extrapolation is used to verify that the 25·0 m solution could be considered spatially grid-converged. The extrapolation is performed using the 50·0 and 25·0 m solutions made with Δt = constant to produce an extrapolated solution that is $O(4)$-accurate in space (remember that the REFC model is $O(2)$-accurate in space). The formula for extrapolation is developed following Conte and de Boor[16] and Evans and Paolucci[17] by assuming that an exact value of a dependent variable ϕ can be found from

$$\phi = \phi_i + \left(C_2 \frac{\Delta x^2}{2!} + C_4 \frac{\Delta x^4}{4!} + \text{higher-order terms} \right),$$

where ϕ_i is the result of a computation using a second-order space scheme, and C_2 and C_4 are functions of higher-order derivatives. With two numerical solutions available (denoted below by subscripts a and b), one made with higher resolution than the other, two approximations for an exact value of ϕ can be found:

$$\phi = \phi_a + \left(C_2 \frac{(50{\cdot}0)^2}{2!} + C_4 \frac{\Delta x^4}{4!} + \cdots \right) \quad \text{(based on the less accurate solution)}$$

and

$$\phi = \phi_b + \left(C_2 \frac{(25{\cdot}0)^2}{2!} + C_4 \frac{\Delta x^4}{4!} + \cdots \right) \quad \text{(based on the more accurate solution).}$$

By assuming that C_2 and C_4 are nearly constant, which is an acceptable approximation for solutions that are converging similarly, an extrapolated value of ϕ can be computed that is Δx^4-accurate in space. This is accomplished by eliminating the terms in C_2, which results in

$$\phi_e = \phi_b + \tfrac{1}{3}(\phi_b - \phi_a),$$

where ϕ_e is the extrapolated value.

The errors in the 25·0 m REFC solution, shown in Table I as the quantity of the difference between the 25·0 m REFC solution and the extrapolated solution divided by the extrapolated solution $[(\phi_{25} - \phi_e)/\phi_e]$, indicate that the maximums and minimums are typically within 0·0001–0·001 of the $O(4)$ in space extrapolated solution. These results suggest that the 25·0 m reference solution is grid-converged, particularly considering that Leone[18] and Evans and Paolucci[17] used an error criterion of 0·01–0·02 to indicate grid convergence in benchmark solutions of their test problem.

The temporal truncation errors are also examined by integrating the REFC model to 900 s with various time steps using a constant spatial resolution. (This is done for resolutions of 50·0, 100·0 and 200·0 m.) The time steps used are $\Delta t = 1{\cdot}5625 \times 10^{-2}$, $3{\cdot}125 \times 10^{-2}$, $6{\cdot}25 \times 10^{-2}$, $12{\cdot}5 \times 10^{-2}$ and $25{\cdot}0 \times 10^{-2}$ s. These time steps are consistent with Δt = constant times δ, where $\delta = 12{\cdot}5$, 25·0, 50·0, 100·0 and 200·0 m (note that $\Delta t = 3{\cdot}125 \times 10^{-2}$ is the time step used for the 25·0 m REFC solution). The L_2 norms for the solutions at a given resolution are computed using

Table I. Results from Richardson extrapolation in terms of $[(\phi_{25}-\phi_e)/\phi_e]$, where ϕ_{25} is a value from the 25·0 m reference solution and ϕ_e is a value from the extrapolated solution

Variable	Reference solution vs. $O(4)$ in space extrapolation solution	Reference solution vs. $O(2)$ in time extrapolation solution
u_{max}	0·0003405	0·0007890
u_{min}	0·0001833	0·0001633
w_{max}	0·0002089	0·0042070
w_{min}	0·0001137	0·0014934
θ'_{max}	0·0000000	0·0000000
θ'_{min}	0·0008252	0·0036280

a solution made with the same resolution and $\Delta t = 1{\cdot}5625 \times 10^{-2} =$ constant times 12·5 m as the reference solution. The results of these computations are plotted in Figure 4 such that, for example, the 200·0 m resolution solution made using a time step consistent with $\Delta t =$ constant times 25·0 m is plotted with an abscissa consistent with 25·0 m resolution. By plotting the errors in this manner, it can be seen that the L_2 norms of the θ' solutions, for a given resolution, contain temporal truncation errors that are nearly an order of magnitude smaller than those due to spatial truncation errors. Notice that the magnitude of the time truncation errors becomes smaller at higher spatial resolutions. Simple extrapolation of the 200·0, 100·0 and 50·0 m time truncation errors suggest that the time truncation errors in the 25·0 m reference solution are similarly small. Also, it can be seen that the time truncation errors improve at about $O(1)$, consistent with that expected for an $O(2)$ scheme with a time filter (e.g. it can easily be shown that an $O(2)$ time scheme, modified by using the Asselin time filter, becomes an $O(1)$ scheme). The small time truncation errors are not surprising since the REFC model was integrated with a fully explicit numerical technique. This required a fairly small time step in order to maintain numerical stability for the fast moving sound waves (e.g. $c_s = 347$ m s^{-1} at $z = 0$). This speed is about an order of magnitude greater than for the physical processes of interest in density current dynamics and, correspondingly, the time scale for the sound waves is about an order of magnitude less.

Richardson extrapolation is also performed to compute a solution that is $O(2)$-accurate in time (i.e. $O(2)$-accurate in time considering the effects of the Asselin time filter; otherwise, the time extrapolated solution would be $O(4)$-accurate) using an additional 25·0 m solution made with the REFC model and a time step of half that used to obtain the 25·0 m reference solution. The results of the time extrapolation, which are provided in Table I, show that the maximums and minimums in the 25·0 m reference solution are within 0·002–0·04 of the $O(2)$ in time extrapolated solution.

To summarize, the results of the L_2 norm calculations and the Richardson extrapolation strongly suggest that the 25·0 m reference solution is grid-converged, at least for the purposes of this paper.

4. COMPARISON SOLUTIONS

Participants of the workshop used their chosen numerical method(s) to simulate the density current test problem using 100·0, 200·0 and 400·0 m resolution. At these resolutions, the flow features of the test problem were, respectively, adequately resolved, marginally resolved and poorly resolved by the REFC model relative to the 25·0 m reference solution. References for the

Table II. Summary of solutions received after the workshop: model methods and references (see text for discussion) (for the AFD and FD model, $N = 2, 4, 6, 8$ and 10)

Participant	Method	Acronym	References
Straka	$O(N)$ finite difference (all derivatives)	AFD (order)	Purser and Leslie[19]
Straka	$O(N)$ finite difference (first derivatives)	FD (order)	Purser and Leslie[19]
Chan	Finite element	FE	Gresho *et al.*,[20,21] Chan *et al.*[22]
Xue	Flux-corrected transport	FCT	Zaleszak,[23] Xue *et al.*[24]
Straka–Anderson	Full local spectral	FLS	Straka and Anderson,[25] Straka *et al.*,[26] Anderson[27]
Hawley	Monotonic upstream	MUa	Finn and Hawley[28]
Wicker–Wilhelmson	Monotonic upstream (scalars)	MUPL	Wicker[29]
Fulton	Spectral	SPEC	Fulton and Shubert,[30] Fulton[31]
Carpenter–Droegemeier	Piecewise parabolic method	PPM	Carpenter *et al.*[32]
Straka	Flux centred	REFC	Droegemeier and Wilhelmson,[6] Droegemeier and Davis-Jones[10]
Straka	Quadratic conserving	REFQ	Matsuno,[13] Kurihara and Holloway[14]
Norman/Stone	Monotonic upstream	MUb	Stone *et al.*[5]
Tripoli	Sixth-order Crowley	CROW	Trembeck *et al.*[33]
Tripoli	Enstropy—energy conserving (velocity); sixth-order Crowley (scalars)	ENST	Tripoli[34]

Table III. Summary of solutions received after the workshop: order of numerical methods used by models (see text for discussion; NM = not meaningful) (for the AFD and FD model, $N = 2, 4, 6, 8$ and 10)

Participant	Method	Accuracy of advection	Pressure solver	Accuracy of pressure	Accuracy of diffusion	Grid staggering (see text)
		space/time		space/time	space/time	
Straka	AFD ($O(N)$)	10/2	Quasi-compressible	10/2	10/1	Unstaggered
Straka	FD ($O(N)$)	even $O(N)/2$	Quasi-compressible	even $O(N)/2$	2/1	Unstaggered
Chan	FE	2/2	Generalized anelastic	2/NM	2/1	Pressure is staggered
Xue	FCT	2/2	Compressible	2/1	2/1	Staggered
Straka–Anderson	FLS	10/2	Quasi-compressible	10/2	2/1	Unstaggered
Hawley	MUa	1/1	Anelastic	2/NM	2/1	
Wicker–Wilhelmson	MUPL	3/1 scalar 2/2 velocity	Quasi-compressible	2/2	2/1	Staggered
Fulton	SPEC	spectral/2	Anelastic	2/NM	2/1	Unstaggered
Carpenter–Droegemeier	PPM	3/1	Compressible	2/1	2/1	Unstaggered
Straka	REFC	2/2	Compressible	2/2	2/1	Unstaggered
Straka	REFQ	2/2	Quasi-compressible	2/2	2/1	Unstaggered
Straka	REFS	2/2	Compressible	2/2	2/1	Staggered
Norman/Stone	MUb	3/1	Compressible	2/1	2/1	Staggered
Tripoli	CROW	6/1	Quasi-compressible	2/1	2/1	Staggered
Tripoli	ENST	6/1 scalar 2/2 velocity	Quasi-compressible	2/2	2/1	Staggered

various numerical methods that were discussed and used at the workshop are summarized in Table II. Additional information about the order of accuracy of the numerical techniques, grid staggering and system of equations used is summarized in Table III. The definitions proposed by Arakawa and Lamb[11] are used to describe grid staggering. For example, all variables are co-located on the unstaggered grid (Arakawa A-grid), while velocity components are centred on the normal edges of grid zones and scalar variables are centred in the grid zones on the staggered grid (Arakawa C-grid).

To begin the discussion of the comparisons, results of the θ' solutions at 900 s for grid resolutions of 400·0, 200·0 and 100·0 m from the FLS, PPM and MUPL models (those of the authors') are shown in Figure 5. Notice that the θ' solutions at 400·0 m resolution show little resemblance to the reference solution. At 200·0 m, the FLS model appears to have captured all of the basic characteristics of the reference solution, including the phase speed of the density current front. However, the solution is plagued by numerical 'noise' problems with what is similar to 'spectral blocking'. The PPM and MUPL models do not suffer from this problem, but they are dissipative, and phase speeds for higher wave numbers are too slow. With 100·0 m resolution, the details in the solutions made with the different models are quite similar. Additional simulations with the FLS and MUPL models using 50·0 m resolution (not shown) produce solutions that contain the finest details of the flow seen in the reference solution (no 50·0 m solution was made with the PPM model).

The θ' solutions at 900 s from the 100·0 and 200·0 m resolution simulations for all of the results submitted after the workshop are shown in Figure 6. As can be seen in Figure 6, all of the methods are capable of correctly reproducing the essence of all of the important physics of the flow in the test problem when the resolution is reduced to 100·0 m. Many of the solutions using 100·0 m resolution are very good; however, there are significant quantitative and qualitative differences between some of the solutions and the 25·0 m reference solution. Most notably, the full development of the leading Kelvin–Helmholtz rotor and phase speed of the density current front are not well simulated with some of the numerical methods. For a modest 200·0 m spatial resolution, differences amongst the solutions are quite noticeable. These solutions are shown because, in modelling complex fluid flows, the spatial resolution is often 'just adequate' due to computational constraints, especially in three dimensions. The differences can be attributed to the particular system of equations solved and to the different properties of the various numerical techniques including order of accuracy, monotonicity and conservation. When the resolution is decreased to 400·0 m, most of the solutions show little or no resemblance to the reference solution (not shown). In addition, some of the models are numerically unstable at 400·0 m resolution (SPEC and high-order FD models).

In processing the results from the workshop, an attempt was made to compute L_2 norms for all of the solutions submitted using the 25·0 m reference solution as the true solution. However, differences in the way that pressure was solved in the various models led to enough differences in the solutions that meaningful comparisons could not be made. To help demonstrate this problem, a 25·0 m resolution reference solution was made using a quasi-compressible version of the compressible reference model. (The quasi-compressible reference model, hereafter referred to as the REFQ model, was integrated with a pseudo sound speed of 150·0 m s^{-1}.) As an example of the sensitivity of the error analyses to different reference solutions, the L_2 norm was 0·45°C for the 100·0 m quasi-compressible FLS θ' solution when compared to the REFC reference solution, and 0·12°C when compared to the REFQ reference solution. In contrast, the PPM model used a compressible system of equations that was similar to the compressible system used in the REFC model. As a result, the L_2 norm was 0·20°C for the 100·0 m resolution PPM θ' solution when compared to the REFC reference solution, and 0·46°C when compared to the REFQ reference

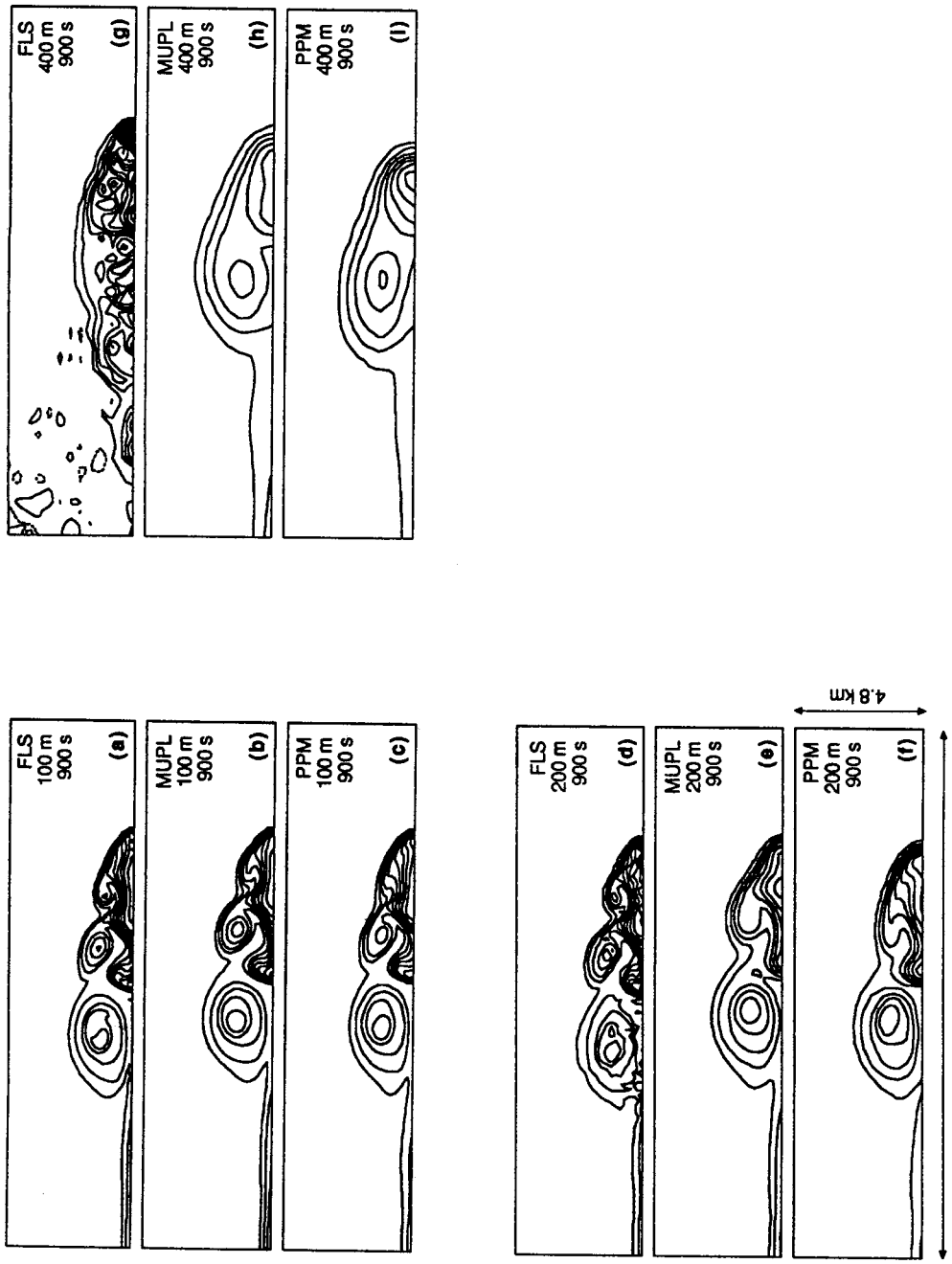

Figure 5. Plots of θ' at 900 s for 100·0, 200·0 and 400·0 m resolution solutions from the FLS (a, d, g), MUPL (b, e, h) and PPM (c, f, i) models. Contour interval (CI) is 1°C (as in Figure 1)

solution. In general, it was found that solutions made with compressible systems converged to the REFC reference solution, while solutions made with quasi-compressible systems (e.g. MUPL) converged to the REFQ reference solution.

Several quantitative measures for each of the submitted solutions were compared with the reference solution, including the location of the density current front (chosen arbitrarily to be the −1°C contour), coldest and warmest θ', total sum of θ', positive and negative contributions to the total θ', total θ'^2 ($\sum \theta'^2$), total enstrophy ($\sum \zeta^2$, where $\zeta = \nabla \times \mathbf{V}$) and total specific kinetic energy ($\sum 0{\cdot}5(u^2 + w^2)$). Numerical values of these quantities for the 200·0 m solutions are shown in Table IV, and are discussed below along with those from the 100·0 and 400·0 m solutions. The numerical values shown in Table IV for the 25·0 m reference solution are from sampling the reference solution at 200·0 m resolution.

The best simulations of the location of the density current front were obtained, as expected, from models with the highest-order schemes. The second-order FCT scheme also performed exceptionally well, especially at coarse resolutions. The worst phase speed errors were associated with the upstream and lower-order finite difference schemes. At 100·0 m resolution, nearly all of the schemes predicted the front location with, at most, 4 per cent error. At 400·0 m resolution, front speed errors varied from 2 to 24 per cent (JFH and REFC solutions, respectively).

The most accurate simulations of total specific kinetic energy and the total enstrophy were obtained with the higher-order models. At 100·0 m resolution, most of the models predicted the total specific kinetic energy to within 2–4 per cent, with some as accurate as 0·5 per cent (FLS). While none of the schemes performed very well at 400·0 m resolution, some were clearly better than others for the given problem. In general, the higher-order FD models, the FLS model and the SPEC model all did quite well at predicting total enstrophy and total specific kinetic energy. In comparison, the upstream and monotonic schemes were quite damped and did not perform as well. However, these solutions contained very little, if any, numerical noise. Note that the higher values of total specific kinetic energy and total enstrophy with the REFC and REFQ models at coarser resolutions were due to high spatial frequencies, that tended to develop with centred-in-space schemes.

The values of minimum θ' values were in error by 0·1–76 per cent in the 100·0 m resolution solutions to more than 1400 per cent at 400·0 m resolution solution. Typically, though, the errors in minimum θ' were closer to 50 per cent in the 400·0 m solutions. The smallest error in minimum θ' using 400·0 m resolution was 6·4 per cent with the FCT model. As expected, the monotonic and upstream methods generally underpredicted the coldest temperatures (too warm), total θ' and $\sum \theta'^2$, especially at coarser resolutions. This correlates well with the smaller magnitudes of kinematic measures for these models, as smaller perturbation potential temperature amplitudes tended to indicate weaker mean flows. The other schemes, such as the centred-in-space and spectral methods generally overpredicted the coldest temperatures (too cold), total θ' and $\sum \theta'^2$, again at the coarser resolutions. This correlates well with the larger magnitudes of kinematic measures found with these schemes, as larger perturbation potential temperature amplitudes tended to indicate stronger mean flows. Finally, it should be noted that very large spurious positive values of θ' ($\theta' > 4$°C) developed in association with poorly resolved sharp gradients of θ' in the coarse resolution simulations made using centred-in-space schemes.

As stated above, solutions of the test problem could have been computed using various approximations of the compressible system of equations and various grid meshes. When reference solutions were made with the REFC model, the REFQ model and a fully compressible model on a staggered grid (Arakawa C-grid, REFS model), subtle differences were found. At first glance, the θ' solutions from the REFC, REFQ and REFS models seem quite similar (Figure 7). However, there are local differences that exceed 50 per cent. An example of this is clearly seen in Figure 7(d),

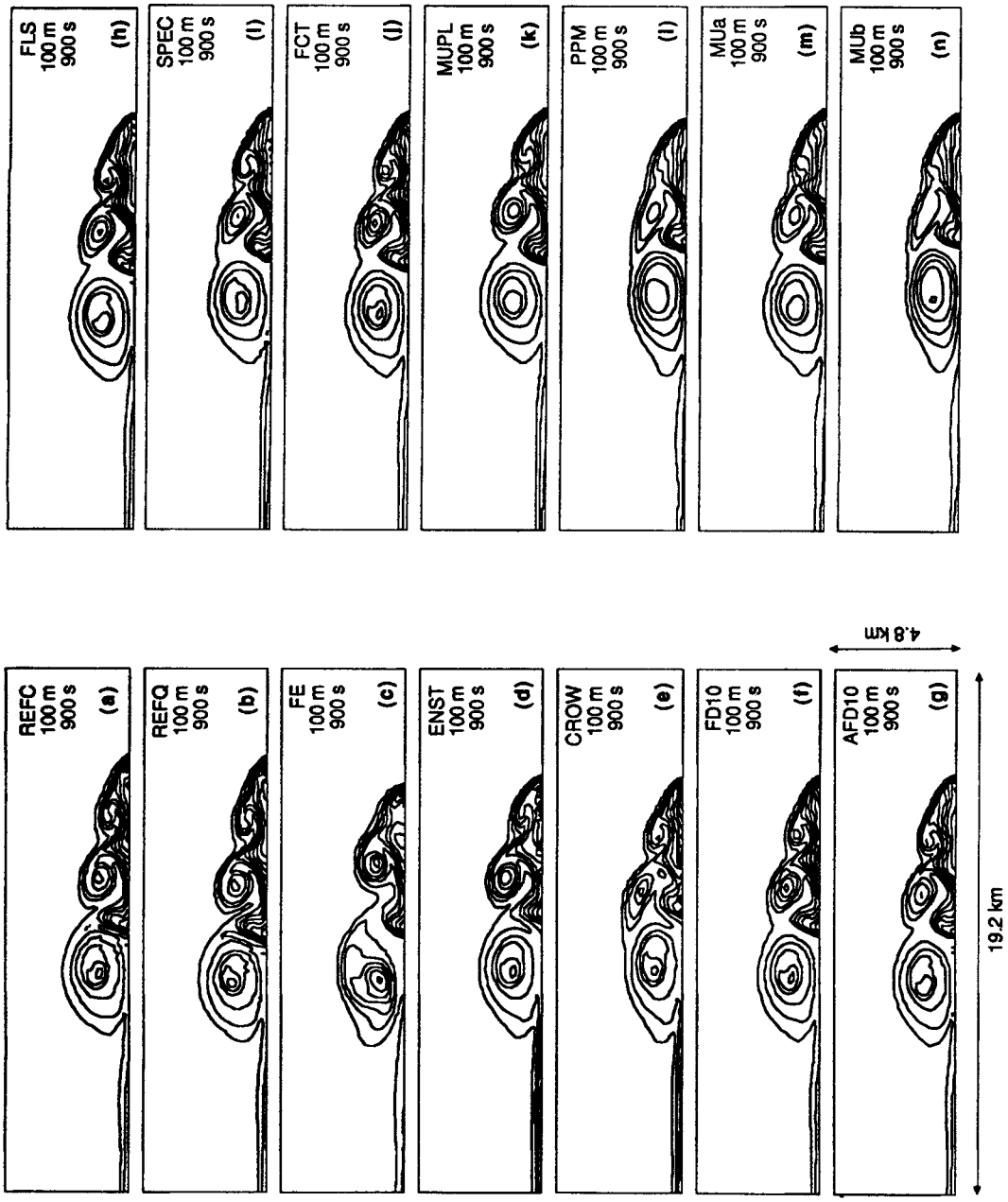
REFC 100 m 900 s (a)
REFQ 100 m 900 s (b)
FE 100 m 900 s (c)
ENST 100 m 900 s (d)
CROW 100 m 900 s (e)
FD10 100 m 900 s (f)
AFD10 100 m 900 s (g)
FLS 100 m 900 s (h)
SPEC 100 m 900 s (i)
FCT 100 m 900 s (j)
MUPL 100 m 900 s (k)
PPM 100 m 900 s (l)
MUa 100 m 900 s (m)
MUb 100 m 900 s (n)
4.8 km
19.2 km

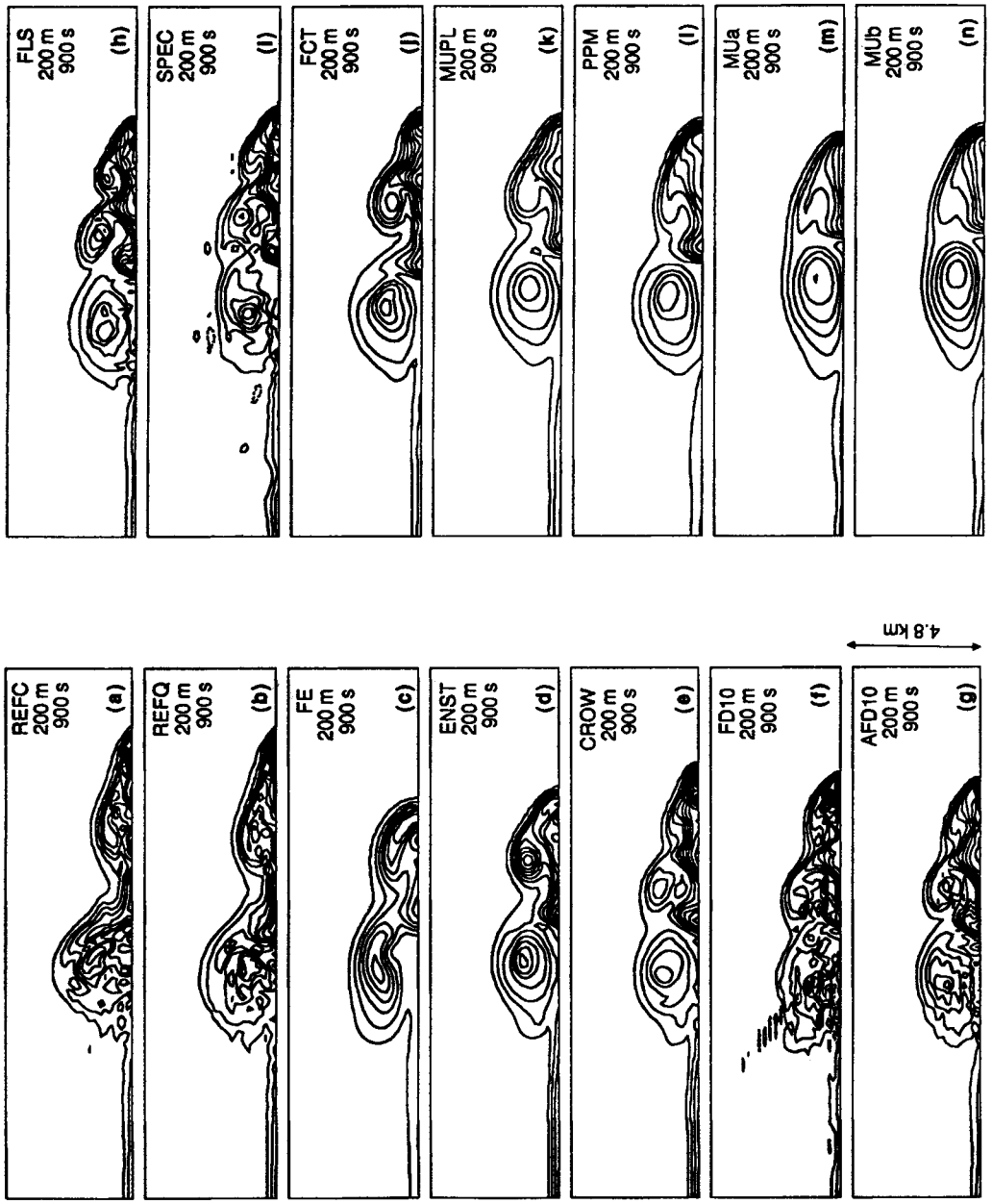

Figure 6. Plots of θ' at 900 s for the 100·0 and 200·0 m solutions from all of the submitted results. Acronym definitions are shown in Table II. Contour interval (CI) is 1°C (as in Figure 1)

Table IV. Statistics for the 200 m simulations (see text for discussion)

Method	Front location (m from $x=0$)	$\sum\theta'$ (K)	$\sum\theta'$ (for $\theta'>0$) (K)	$\sum\theta'$ (for $\theta'<0$) (K)	$\sum$KE ($m^2 s^{-2}$)	$\sum\zeta^2$ (s^{-2})	θ_{max} (K)	θ_{min} (K)	$\sum\theta'^2$ (K^2)
AFD10	15175·97	−1522·02	10·560	−1532·580	89523·45	0·28532	0·60831	−16·5861	7512·49
FD02	Unstable	Unstable	Unstable	Unstable	Unstable	Unstable	Unstable	Unstable	Unstable
FD04	Unstable	Unstable	Unstable	Unstable	Unstable	Unstable	Unstable	Unstable	Unstable
FD06	15205·56	−1539·57	50·374	−1589·94	90826·3	0·36354	1·3727	−21·7034	7455·34
FD08	15312·25	−1547·30	50·798	−1598·10	90437·8	0·33477	1·3996	−20·5390	7951·94
FD10	15344·90	−1544·49	47·255	−1591·74	90204·8	0·32898	1·1637	−21·5842	8357·94
FE	14532·76	−1358·66	3·7766	−1362·44	72393·9	0·19958	0·18906	−8·43701	5320·12
FCT	15426·02	−1406·75	0·0000	−1406·75	81664·5	0·24736	0·00000	−10·1065	5869·83
FLS	15174·20	−1518·09	12·794	−1530·88	90265·7	0·29972	0·67697	−14·1625	7509·47
MUa	14566·62	−1292·61	55·030	−1347·64	82024·8	0·21410	0·18953	−7·73373	5093·57
MUPL	15188·39	−1449·04	0·0000	−1449·04	95565·9	0·24115	0·00000	−7·82435	5355·54
SPEC	15574·60	−1352·39	125·35	−1477·74	91483·2	0·32510	0·69894	−11·7825	6039·57
PPM	15027·97	−1408·65	1·5801	−1410·23	83364·8	0·20404	0·02200	−8·31125	5665·45
REFC	17069·85	−1467·79	9·2917	−1477·08	89156·9	0·37020	0·56449	−10·9667	5858·15
REFQ	16998·44	−1562·44	11·137	−1573·58	93203·0	0·38867	0·61230	−11·6727	6832·78
MUb	14853·97	−1403·14	69·800	−1472·95	83188·0	0·20420	0·43787	−7·90158	6037·31
CROW	15745·98	−1597·09	4·6649	−1601·75	85592·6	0·25326	0·10216	−20·5178	7833·42
ENST	14801·46	−1549·51	1·7945	−1551·30	85804·0	0·23555	0·05656	−9·96810	6588·00
REFC25	15537·44	−1427·10	0·0000	−1427·10	91580·7	0·34306	0·00000	−9·77375	6613·62
REFQ25	15509·17	−1512·80	0·0000	−1512·80	90699·8	0·37140	0·00000	−10·0000	7395·26

Note: REFC25 and REFQ25 are the 25 m compressible and quasi-compressible reference solutions sampled at 200 m.

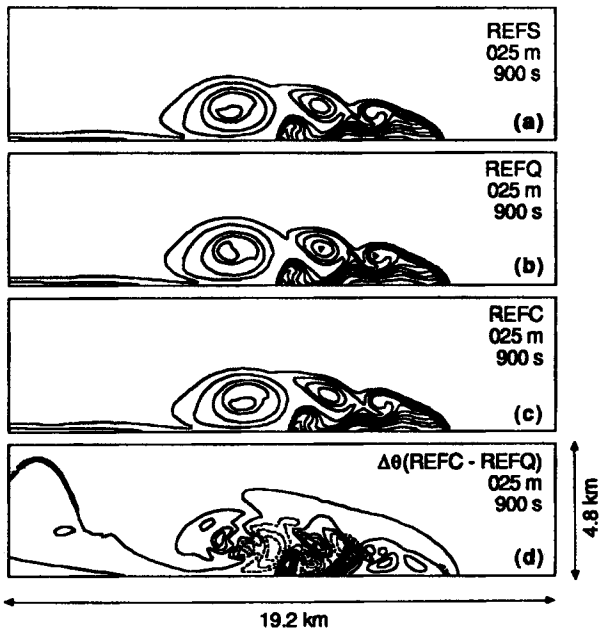

Figure 7. Plots of θ' at 900 s for the 25·0 m solutions from the (a) staggered compressible reference model (REFS), (b) the quasi-compressible reference model (REFQ) and (c) the compressible reference model (REFC). The difference field of θ' (CI = 0·5°C) between the 25·0 m solutions from the REFC and REFQ models is shown in (d) (as in Figure 1)

Table V. Comparison of maximums and minimums of p, θ', u and w at 900 s for the 25 m solutions from (a) the compressible reference model using an unstaggered grid (REFC), (b) the compressible reference model using a staggered grid (REFS) and (c) the quasi-compressible model with unstaggered grid (REFQ)

Variable	REFC	REFS	REFQ
p'_{max} (mb)	2·87	2·49	1·74
p'_{min} (mb)	−5·14	−5·55	−5·21
θ'_{max} (K)	0·00	0·00	0·00
θ'_{min} (K)	−9·77	−9·77	−10·00
u_{max} (m s^{-1})	36·46	35·02	34·72
u_{min} (m s^{-1})	−15·19	−16·32	−15·31
w_{max} (m s^{-1})	12·93	13·28	13·04
w_{min} (m s^{-1})	−15·95	−16·11	−16·89

Table VI. Zone cycles (thousands) per second and total central processor unit (CPU) time (s) for selected models on the NCSA's Cray-XMP/48 and Cray-2/128

Method (machine)	64 × 16 (400 m)	128 × 32 (200 m)	256 × 64 (100 m)
FCT (Cray-2)	53 (6)	63 (80)	67 (180)
FE (Cray-2)	37 (3)	49 (15)	51 (116)
FLS (Cray-2)	34 (20)	39 (120)	42 (1200)
MUa (Cray-XMP)	149 (18)	169 (126)	190 (900)
MUb (Cray-2)	76 (21)	102 (102)	156 (658)
MUPL (Cray-2)	310 (3)	440 (15)	525 (112)
PPM (Cray-XMP)	68 (21)	90 (127)	98 (938)
REFC (Cray-2)	187 (10)	214 (69)	230 (512)
REFQ (Cray-2)	208 (4)	223 (133)	240 (246)
SPEC (Cray-XMP)	14 (12)	16 (45)	16 (187)

which shows the differences between the 25·0 m resolution REFC and REFQ θ' solutions. These discrepancies are associated with differences in the phase speed of the leading edge of the density current, and the movement of the trailing rotors. There are also differences of 0–5 per cent in the global maximums and minimums of θ', p', u and w (Table V). While these differences are smaller than at coarser grid resolutions, it is not known if they would continue to decrease at resolutions smaller than 25·0 m. Interestingly, these are larger than the differences found in the Richardson extrapolation done with the solutions from the REFC model.

Finally, many participants of the workshop provided timings for their models, in terms of grid zone cycles per second, based on simulations made on NCSA's Cray-2/128 and Cray-XMP/48 (Table VI). As can be seen, most models are up to 40 per cent faster with refined resolution. This is due to the more efficient vectorization of longer loops in the higher-resolution simulations. Another important point is that the speeds of the individual models differed by up to an order of magnitude. These timings are somewhat misleading, though, since some of the slower codes, such as the SPEC model, can be run with a very long time step and are quite competitive (in terms of total central processor unit time) with some of the other schemes. Unfortunately, a more

comprehensive comparison of accuracy versus efficiency of different numerical techniques could not be made with the information made available. This is due, in part, to the fact that such a comparison was not a primary goal of the workshop.

5. CONCLUDING REMARKS

In summary, the follwing statements can be made regarding the results from the simulations presented at the workshop:

(1) When the flow was adequately resolved, all of the numerical schemes captured the basic physics of the flow. However, there were still noticeable differences in the timing and location of these flow features, even at very high resolutions. The most accurate solutions, in terms of reproducing the basic features of the flow as described in Section 3, were, in general, those made with high-order and spectral methods. The major problem with the solutions made with the monotonic schemes was that some features of the flow were underdeveloped and moved too slow due to the damping characteristics of these schemes.

(2) When the flow was marginally resolved, there were significant differences between the solutions produced by the various models. For example, the upstream and monotonic models incorrectly simulated two Kelvin–Helmholtz rotors, while higher-order models correctly simulated three Kelvin–Helmholtz rotors. In simulating the basic flow features, the local spectral scheme performed best; however, it had some problems with energy accumulation at the highest spatial wave numbers.

(3) When the flow was poorly resolved, none of the models performed well. However, the models that incorporated damped advection schemes produced coherent (smooth) flow structures, while the models that incorporated higher-order centred schemes produced very noisy solutions. In fact, the solutions made by the local spectral and spectral models were essentially unusable, and some solutions made with high-order finite difference models became unstable.

Overall, it appears that no scheme universally produced the best solutions for all of the resolutions tried. Clearly though, some schemes were better at coarse resolution, while others were better at finer resolutions as described above.

A general result that was reinforced at the workshop was that care must be taken when interpreting the physics described by simulations of non-linear flows with resolutions that might be considered marginal. The results from the marginal resolution simulations, which were described above, clearly demonstrate this in that the evolution of some simulations was considerably different than others. While computers have been developed with enough speed and memory to carry out simulations of most two-dimensional problems with adequate resolution, many three-dimensional simulations are still made with marginal resolution due to computational constraints.

Another result from the workshop was that numerical solutions can be quite sensitive to approximations made to the governing equations (without necessarily influencing the reproduction of the basic physics). For example, simulations made with quasi-compressible systems tended to converge to a reference solution made with a quasi-compressible model, while simulations made with fully compressible systems tended to converge to a reference solution made with a fully compressible model. Because of this, there was considerable difficulty in determining which 25·0 m solution should be used as the reference solution. Furthermore, this precluded a detailed error analysis of all of the solutions submitted after the workshop. For these reasons, it is suggested that participants of similar workshops in the future solve exactly the same system of

equations so that comparisons with a reference solution and with results from other models can be made more quantitatively.

Finally, it was agreed upon at the 'Workshop on Numerical Methods for Solving Nonlinear Flow Problems' that workshops such as the one described in this paper are vital for comparing results from the many numerical techniques that are now available to solve complex fluid flow problems. They also provide a unique opportunity for scientists from various disciplines to interact and convey new information.

ACKNOWLEDGEMENTS

The authors are grateful to Dr. Larry Smarr, Crystal Shaw, Brian Jewett, Gwen Van Gompel, and the many others involved in making this workshop possible. In addition, thanks are due to Kathy Kanak, Dr. Gregory Tripoli, Dr. Steven Chan, Dr. Steven Fulton and two reviewers for their encouragement and candid comments. Finally, we extend our gratitude to Dr. Philip Gresho for encouraging us to write this paper and providing useful suggestions. Support for the workshop was provided by the National Center for Supercomputing Applications (NCSA), the Space Science and Engineering Center at the University of Wisconsin-Madison, and the Center for Analysis and Prediction of Storms. National Science Foundation support for this paper was provided through grants ATM 87-00778 and ATM 88-09862. Time on the Cray-2/128 and Cray-XMP/48 computers was provided at NCSA through a Cray-sponsored University Research and Development Grant. The reference solutions were made on the Cray-2/128 at NCSA and the Alliant/FX8 at the University of Oklahoma-Norman.

REFERENCES

1. R. D. Richtmeyer and K. W. Morton, *Difference Methods for Initial Value Problems*, Interscience, New York, 1967.
2. P. R. Woodward and P. Collela, 'The numerical simulation of two dimensional flow with strong shocks', *J. Comput. Phys.*, **54**, 115–173 (1984).
3. P. M. Gresho and R. I. Sani, 'Introducing four benchmark solutions', *Int. j. numer. methods fluids*, **11**, 951–952 (1990).
4. J. M. Stone and M. L. Norman, 'ZEUS-2D: a radiation magnetohydrodynamics code for astrophysical flow in two space dimensions: I. The hydrodynamic algorithms and tests', *Astrophys. J. Suppl.*, **80**, 753–790 (1992).
5. J. M. Stone, J. F. Hawley, C. R. Evans and M. L. Norman, 'ZEUS-2D: a test suite for magnetohydrodynamical simulations', *Astrophys. J. Suppl.*, **388**, 415–437 (1992).
6. K. K. Droegemeier and R. B. Wilhelmson, 'Numerical simulation of thunderstorm outflow dynamics. Part 1: outflow sensitivity experiments and turbulence dynamics', *J. Atmos. Sci.*, **44**, 1180–1210 (1987).
7. Y. Ogura and N. A. Phillips, 'A scale analysis of deep and shallow convection in the atmosphere', *J. Atmos. Sci.*, **19**, 173–179 (1962).
8. A. J. Chorin, 'A numerical method for solving incompressible flow problems', *J. Comput. Phys.*, **2**, 12–16 (1967).
9. J. R. Anderson, K. K. Droegemeier and R. B. Wilhelmson, 'Simulation of the thunderstorm subcloud environment', preprints, in *Proc. 14th Conf. on Severe Local Storms*, Indianapolis, Indiana, Am. Meteorol. Soc., 1985, pp. 147–150.
10. K. K. Droegemeier and R. Davis-Jones, 'Simulations of thunderstorm microbursts with a super-compressible numerical model', preprints, in *Proc. 5th Int. Conf. on Numer. Methods in Laminar and Turbulent Flow*, Montreal, Quebec, 1987, pp. 1386–1397.
11. A. Arakawa and V. R. Lamb, 'Computational design of the basic dynamical processes of the UCLA general circulation model', in *Methods of Computational Physics*, Vol. 17, Academic Press, New York, 1977, pp. 174–265.
12. R. Asselin, 'Frequency filter for time integrations', *Mon. Weather Rev.*, **100**, 487–490 (1972).
13. T. Matsuno, 'Numerical integrations of primitive equations by use of a simulated backward difference method', *J. Meteorol. Soc. Japan*, **44**, 76–84 (1966).
14. Y. Kurihara and J. Holloway, 'Numerical integrations of a nine-level global primitive equation model formulated by the box method', *Mon. Weather Rev.*, **118**, 586–612 (1967).
15. K. K. Droegemeier and R. B. Wilhelmson, 'Kelvin–Helmholtz instability in a numerically simulated thunderstorm outflow', *Bull. Am. Meteorol. Soc.*, **67**, 416–417 (1986).
16. S. D. Conte and C. de Boor, *Elementary Numerical Analysis. An Algorithmic Approach*, 3rd edn, McGraw-Hill, New York, 1980.
17. G. Evans and S. Paolucci, 'The thermoconvective instability of plane poiseuille flow heated from below: a proposed benchmark solution for open boundary flows', *Int. j. numer. methods fluids*, **11**, 1001–1013 (1990).

18. J. M. Leone, Jr., 'Open boundary condition symposium benchmark solution: stratified flow over a backward-facing step', *Int. j. numer. methods fluids*, **11**, 969–984 (1990).
19. R. J. Purser and L. M. Leslie, 'A semi-implicit, semi-Lagrangian finite difference scheme using high-order differencing on a nonstaggered grid', *Mon. Weather Rev.*, **116**, 2069–2080 (1988).
20. P. M. Gresho, S. T. Chan, R. L. Lee and C. D. Upson, 'A modified finite element method for solving the time-dependent, incompressible Navier–Stokes equations. Part 1: theory', *Int. j. numer. methods fluids*, **4**, 557–598 (1984a).
21. P. M. Gresho, S. T. Chan, R. L. Lee and C. D. Upson, 'A modified finite element method for solving the time-dependent, incompressible Navier–Stokes equations. Part 2: applications', *Int. j. numer. methods fluids*, **4**, 619–640 (1984b).
22. S. T. Chan, D. L. Ermak and L. K. Morris, 'FEM3 model simulation of selected Thorny Island Phase I trials', *J. Haz. Materials*, **16**, 267–292 (1987).
23. S. T. Zalesak, 'Fully multidimensional flux-corrected transport algorithms for fluids', *J. Comput. Phys.*, **31**, 335–362 (1979).
24. M. Xue and A. J. Thorpe, 'A mesoscale numerical model using the nonhydrostatic pressure-based sigma coordinate equations: model experiments with dry mountain flows', *Mon. Weather Rev.*, **119**, 1168–1185 (1991).
25. J. M. Straka and J. R. Anderson, 'Extension and application of a local, minimum aliasing method to multi-dimensional problems in limited area domains', *Mon. Weather Rev.* in press (1993).
26. J. M. Straka, R. B. Wilhelmson, L. J. Wicker, K. K. Droegemeier and J. R. Anderson, 'Workshop on numerical methods for solving nonlinear flow problems', preprints, in *Proc. 9th Conf. on Numerical Weather Prediction Conference*, Denver, Colorado, Amer. Meteorol. Soc., 1991, pp. 274–278.
27. J. R. Anderson, 'A local, minimum aliasing method for use in nonlinear numerical models', *Mon. Weather Rev.*, **117**, 1369–1379 (1989).
28. L. S. Finn and J. F. Hawley, 'Finite differencing the non-linear continuity equation: velocity corrected transport', CRSR 928, Cornell University, Center for Radiophysics and Space Research. Ithaca, New York, 1989.
29. L. J. Wicker, 'A numerical simulation of a tornado-scale vortex in a three-dimensional cloud model', *Ph.D. Thesis*, University of Illinois at Urbana-Champaign, 1990.
30. S. R. Fulton and W. H. Shubert, 'Chebyshev spectral methods for limited area models. Part I: model problem analysis', *Mon. Weather Rev.*, **115**, 1940–1965 (1987).
31. S. R. Fulton, 'A simple anelastic spectral model. A workshop on the comparison of numerical methods for solving nonlinear flows', *J. Comput. Phys.*, (submitted).
32. R. L. Carpenter, Jr., K. K. Droegemeier, P. R. Woodward and C. E. Hane, 'Application of the piecewise parabolic method (PPM) to meteorological modeling', *Mon. Weather Rev.*, **118**, 586–612 (1990).
33. C. J. Tremback, J. Powell, W. R. Cotton and R. A. Pielke, 'The forward-in-time upstream advection scheme: extensions to higher orders', *Mon. Weather Rev.*, **115**, 540–555 (1987).
34. G. J. Tripoli, 'A non-hydrostatic mesoscale model designed to simulate scale interaction', *Mon. Weather Rev.*, **120**, 1342–1359 (1992).